ACS Sustainable Chemistry & Engineering

Research Article

pubs.acs.org/journal/ascecg

Multifunctionality of Silicified Nanoshells at Cell Interfaces of *Oryza sativa*

Jie Ma, Xiuqing Zhang, Wenjun Zhang, and Lijun Wang*

College of Resources and Environment, Huazhong Agricultural University, Wuhan 430070, China

Supporting Information

ABSTRACT: The mimic and design of artificial nanoshell materials on individual cells have been explored in microbial and mammalian cells, and these synthetic interfacial materials can confer new and unique properties on living cells to resist various environmental stresses. However, no attempts have been made toward chemical nanoencapsulation of higher plant cells. Here, we cultivated rice (*Oryza sativa*) single cells whose cell walls were silicified identically by mimicking diatom biomineralization. Results show that the silica nanoshell at the cell interface is effective at adsorbing cadmium (Cd^{2+}) ions by in situ noninvasive microtest technology to quantitatively measure Cd^{2+} ion fluxes, rapidly sequestering and immobilizing Cd ions in the silicified cell walls with adsorption fluxes 6- to 10-times greater than those of the unsilicified cell walls. This, therefore, confers increased Cd tolerance by inhibiting Cd ion uptake into cells. In addition, using in situ atomic force microscopy to probe cell mechanical properties, the cell walls are remarkably strong by virtue of the material properties of the silica nanoshells that physically protects the cells against mechanical challenges. Chemically silicified cells may have acquired a multifunctionality of co-optimized mechanical protection and heavy metal detoxification by organic−inorganic composite materials of the silicified cell walls.

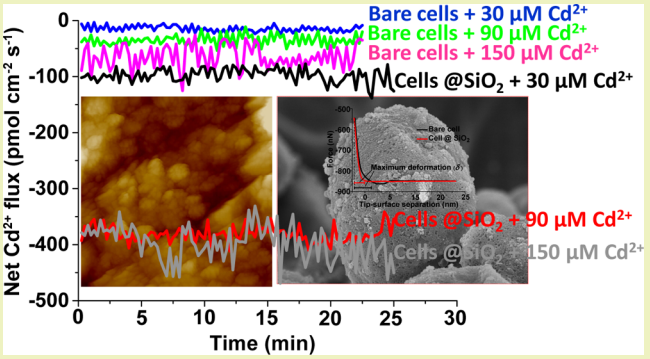

KEYWORDS: *Silica, Cadmium, Cell−mineral interface, Oryza sativa*

INTRODUCTION

Inspired by the formation of shells in natural living organisms,[1−4] researchers have coated different species of microbial or mammalian cells with artificial nanoshells using various (bio)chemical modification methods, such as layer-by-layer assembly, ion binding, self-formation, and genetic engineering.[5,6] Accordingly, different materials including polyelectrolyte multilayer films, calcium phosphate, lanthanide phosphate, and silica have been used for the surface modification and coating depending on the cell type or purpose of the application.[7] The coated cells may acquire new abilities (cell viability maintenance, storage, and thermal stability[6,8]) under environmental stresses.

The previous studies of bioinspired surface coating mainly focused on bacteria, yeast, and mammalian cells.[8−10] However, the potential applications of artificially coated cell-in-shell hybrids have rarely been reported for higher plant cells. Crops such as rice (*Oryza sativa*) are domesticated and cultivated as a staple cereal grain for a major source of nutrition for approximately two-thirds of mankind.[11] However, rice and other crops growing on cadmium (Cd)-contaminated soils accumulate high concentrations of Cd,[12] resulting in growth retardation and biomass reduction[13] as well as human health risks.[14] Moreover, the weak mechanical strength can also cause lodging and reduce grain yield.[15] Trade-offs between factors contributing to biomechanics and affecting plant survival under heavy metal stress remain poorly understood due to the whole-plant complexity and a lack of corresponding measurement tools. In the present study, we cultivated rice single cells whose cell walls were silicified identically by mimicking diatom biomineralization in which the formation of silica shells was catalyzed by a polyamine template.[10] Results show that the silica shell is effective at adsorbing cadmium (Cd^{2+}) ions to confer increased Cd tolerance by inhibiting Cd uptake into cells. Moreover, using in situ atomic force microscopy (AFM) to probe cell mechanical properties, the cell walls were remarkably strong by virtue of the material properties of the silica nanoshell that physically protects the cells against mechanical challenges.

EXPERIMENTAL SECTION

Cell Culture. Single cell lines of *Oryza sativa* were obtained from mature seeds.[16] The cells were suspension cultured in 125 mL plastic Erlenmeyer flasks with 40 mL of liquid amino acid (AA) medium (pH 5.9) containing 1 mg/L of 2,4-D (Table S1) and cultivated on a rotary shaker (110 rpm) at 28 °C in the dark. Then, 1.0 mM silicic acid was added in medium as Si nutrient, and the solution was renewed every 5 d for more than 3 months before further treatments.

Received: July 25, 2016
Revised: September 16, 2016
Published: October 3, 2016

DOI: 10.1021/acssuschemeng.6b01736
ACS Sustainable Chem. Eng. 2016, 4, 6792−6799

Silica Mineralization. The silica mineralization was carried out according to an established method.[10] Briefly, the cells were incubated in AA medium in the presence of cationic polyelectrolytes (0.1 mg/mL of PEI, pH 7.0) for 10 min. Then, the cells preadsorbed by poly(ethylenimine) (PEI) were washed by AA and placed in a silicic acid solution, which was formed by hydrolyzing 1.0 M tetramethyl orthosilicate (TMOS) in 1.0 mM HCl (TMOS to AA with 5:95 (v/v) ratio at pH 7.0). After 20 min, the silicified cells were washed to remove unhydrolyzed TMOS and then transferred to AA medium.

Cell Morphology Observations by SEM. Bare cells or silica-coated cells (cells@SiO_2) were placed in the slots of a stub and then immersed frozen in liquid nitrogen. After quickly transferring the samples into the cryopreparation chamber of a cryosystem (PP3010T, Quorum Technologies Ltd., UK), they were cryofractured at −180 °C for cross section observations. Moreover, cells were directly placed on SEM slides and frozen in liquid nitrogen for surface imaging. All samples were sublimated and subsequently sputter-coated with Pt and examined in a field-emission scanning electron microscopy (FE-SEM, SU8000, Hitachi) at an accelerating voltage of 10−20 kV. The FE-SEM is equipped with an energy-dispersive X-ray (EDX) detector for the elemental analyses of Si and Cd distributions in cells using a voltage of 20 kV.

XPS Characterization for the Si and Cd Bonding States. Bare cells or cells@SiO_2 were dried under a vacuum for at least 12 h prior to measurements. The lyophilized cell samples were placed on an aluminum platform for XPS (VG multilab 2000, Thermo VG Scientific; East Grinstead, West Sussex, UK) using Al Kα (1486.6 eV) as the X-ray excitation source at a power of 300 W.[17] To compensate for the surface charging, the neutral C (1s) peak at 284.6 eV was used as a reference for all binding energies, and the background was linearly subtracted.[17] The software Thermal Advantage (http://www.tainstruments.com) was used for data analysis. XPS experiments were repeated at least three times to ensure the reproducibility of results.

AFM Imaging. Bare or @SiO_2 cells were washed with Milli-Q water three times and dropped onto glass coverslips. Then, cells were dried with N_2 gas flow for 24 h before AFM experiments. AFM imaging was acquired in ScanAsyst Air mode using the corresponding Bruker ScanAsyst Air probes (tip radius: 2−12 nm and silicon nitride cantilever; spring constant of 0.4 N/m). For all AFM modes used in our experiment, the scan rate was set to 2 Hz. All AFM measurements were performed on a MultiMode VIII AFM (Bruker, Santa Barbara, CA, USA) with an E scanner in air at room temperature and approximately 50% relative humidity.[18] NanoScope Analysis (Bruker) software was used to analyze AFM images and data. All instrumentation was used and calibrated according to the manufacturer's recommended procedures.

AFM Force Measurements. The mechanical properties were measured using RTESP tips (tip radius of 8 nm and spring constant of 20−80 N/m; Bruker). For quantitative force measurements, the deflection sensitivity (30−35 nm/V) and the precise spring constant (30−60 N/m) of each tip was determined and calibrated prior to the experiments.[18] The deflection of the cantilever is recorded as approach/retrace curve while the tip is descended to the cell surface and pushed against it (approach curve), and then the tip is retracted to its starting position (retrace curve) and moved to the next required pixel of the image. By analyzing the force versus separation curves, quantitative information on deformation and Young's modulus E can be obtained.[19] The Herz model has been used in the majority of studies to evaluate the Young's modulus of cells[20]

$$E = \frac{3}{4}\frac{F(1-\nu^2)}{R^{1/2}\delta^{3/2}} \quad (1)$$

where E represents the Young's modulus of sample, F is the force related to the deformation, υ is the Poisson ratio of the sample (ranging from 0 to 0.5; 0.3 is usually assumed for cell walls that reflects the compressibility of the sample),[21] R is the tip radius, and δ is the maximum deformation defined as the indentation of the tip into the surface and calculated from the point of zero force to the peak force point along the approach curve.

KPFM for Surface Potentials. Bare cells, cells@SiO_2, and cells treated with Cd (90 μM $CdSO_4$ for 20 min) were washed with phosphate-buffered saline (PBS) twice and then with Milli-Q water three times. The samples were dropped onto glass coverslips followed by drying overnight with N_2 gas. The coverslip with cells was placed on a steel AFM sample mounting disk and set at electrical ground for the KPFM measurements.[22] A Multimode EFM cantilever holder (MMEFCH) and conductive AFM tips (MESP) were applied for the KPFM scanning. In KPFM mode, the AFM instrument employed a two-pass procedure whereby the surface topography and the surface potential are simultaneously and independently obtained.[23] In the first pass, the standard tapping mode captured the topographic images, and then the tip was lifted to 50 nm (in this experiment set) above the cell surface while the tapping drive piezo was turned off and both an AC and DC voltage signal were applied directly to the probe tip

$$V_{tip} = \Delta V_{DC} + V_{AC}\sin(\omega t) \quad (2)$$

where ω is the resonant frequency of the cantilever and an oscillating electric force will occur on the cantilever. This causes a vibration of the cantilever with detectable amplitude. To keep the physical oscillation amplitude of the cantilever at zero, a feedback loop adjusted the DC voltage difference between the tip and sample ($\Delta V_{DC} = 0$). Consequently, there is no force on the cantilever at frequency ω, and the cantilever oscillation vanishes.[22] The DC voltage applied to the tip was the same as the surface potential (Φ_S).[22−24] Finally, the voltage applied to the probe tip was recorded by the NanoScope V Controller to construct a voltage map of the surface. The surface potential was measured at a minimum of three locations for each cell sample, and at least ten samples of each treatment were measured. A gold surface (PFKPFM-SMPL; Bruker) with a defined work function of ∼5.1 eV was used as a reference to calibrate the surface potential (Φ_S) before and after each potential measurement.[25]

In Situ NMT for Cd Ion Fluxes. Net fluxes of Cd^{2+} were obtained with an ~~NMT system~~, (NMT100 Series, Younger USA) at the NMT Service Center (Xuyue ~~Beijing~~ Sci. & Tech. Co., Ltd. Beijing, China). Manufactured microelectrodes selective for Cd^{2+} with an external tip (inner diameter ∼3 μm) were silanized with tributylchlorosilane, and the tips were backfilled with an ion-selective cocktail (Cd Ionophore I, 20909; Fluka, Buchs, Switzerland). Before and after each Cd^{2+} flux measurement, the microelectrodes were calibrated in measuring solution with 5 and 50 μM Cd^{2+}. Only electrodes with Nernstian slopes >22 mV/decade were used.[26]

Bare and @SiO_2 cells (200 μL) were placed on glass coverslips pretreated with a poly-L-lysine solution and transferred to Petri dishes containing 3 mL of equilibrating solution (0.005 mM $CdSO_4$, 0.1 mM KCl, 0.3 mM 2-(*N*-morpholino)ethanesulfonic acid (MES), and 0.1% sucrose, pH 6.0) for 10 min.[25] The solution was removed and 3 mL of measuring solution (same composition as the equilibrating solution but with 30, 90, or 150 μM $CdSO_4$) was added. The Petri dishes were then placed on the micromanipulator, and the Cd^{2+}-selective microelectrodes were positioned close to the cell surfaces. To record voltage gradients of Cd^{2+} near the cell surface, the microelectrode was moved between two points (period of ∼2 s/point) at a preset distance of 10 μm in a perpendicular direction to the cell surface.[25] The raw data of fluxes (voltage differences, mV) were obtained with the iFluxes/imFluxes 1.0 (~~Younger USA, LLC~~, Amherst, MA 01002, USA) software and exported and converted into the specific ion net fluxes (pmol cm^{-2} s^{-1}) using JCal software (version 3.3, ~~Xu-Yue Sci. & Tech~~; free MS Excel spreadsheet, http://youngerusa.com/jcal). The calculations of net ion fluxes were based on Fick's law of diffusion

$$J = -D_0(dc/dx) \quad (3)$$

where J is the ion flux, D_0 is the ionic diffusion constant of a specific ion, dc is the ion concentration gradient, and dx is the distance that the microelectrode moved between the two points perpendicular to the cell surface.[27] Prior to NMT measurements, the viabilities of *Oryza* single cells before and after silica coating and cells treated with Cd

DOI: 10.1021/acssuschemeng.6b01736
ACS Sustainable Chem. Eng. 2016, 4, 6792−6799

were measured by fluorescein diacetate (FDA)-propidium iodide (PI) double staining. At least six cell samples were measured for each treatment, and their mean values ± SD were presented. The statistical significance of differences in mean values at each point was determined with a Student's *t*-test.

Cell Viability. Fluorescein diacetate (FDA) can be taken up by living cells and converted to a green fluorescein by esterases found exclusively in viable cells. In comparison, the nuclei staining dye propidium iodide (PI) can only pass through disordered areas of the membranes of dead cells and generate red fluorescence by intercalating with the DNA double helix.[17] A fresh FDA-PI solution was made by adding 1 μL of PI and 1 μL of FDA to 98 μL of Milli-Q water. Then, 10 μL of FDA-PI solution was mixed with 90 μL of solution containing cells and incubated for 2 min at room temperature in the dark.[17] The viability of cells treated with PEI, and cells further treated with TMOS, were all examined. Bare cells without any treatment were set as control and washed and filtered following the coating procedure. The experiment was repeated three times, and more than 100 cells were observed in each treatment.

Optical visualization was conducted by an Olympus BX51 light/fluorescence microscope (Tokyo, Japan) equipped with a digital CCD camera (DS-Fil; Nikon, Tokyo, Japan), and images were captured and measured by NIS-ELEMENTS F 3.0 software (Nikon).

Reagents. All reagents were purchased from Sigma-Aldrich unless particularly noted. Ultrahigh purity water, >18 MΩ cm, from a two-step purification treatment including triple distillation (YaR, SZ-93, Shanghai, China) and deionization (Milli-Q, Billerica, MA, USA) was used to prepare all solutions.

RESULTS AND DISCUSSION

Our previous results showed that for suspended cells of rice cultivated in the presence of 0.5−2.0 mM $Si(OH)_4$ in the culture medium, a trace amount of Si was naturally present as a constituent of the cell walls, where it was firmly bound to the cell wall matrix rather than occurring within intra- or extracellular silica deposits,[17] suggesting no evidence of silica formation on cell walls. The spontaneous precipitation of $Si(OH)_4$ on the cell walls requires either a mechanism to concentrate $Si(OH)_4$ above its solubility limit or a process whereby the cell wall surface nucleation is driven primarily by local fluctuations in the interfacial energy, which manifest themselves as reductions in the thermodynamic barrier to silica cluster/oligomer formation specifically at the solution−substrate interface.[28,29] Once a supersaturation with respect to amorphous silica is maintained in xylem,[30] hydrostatic and osmotic forces drive the radial and axial movement of supersaturated $Si(OH)_4$ solutions from xylem, a time-dependent precipitation of silica will eventually occur on cell walls.[31] However, in this suspension cell system, because of the chemical structure of the cell wall of *Oryza sativa*, which consists mainly of negatively charged polysaccharides,[32] spontaneous mineralization and deposition of silica is barely induced.

Inspired by biosilica shell formation of diatom cell walls whose colloidal components were catalyzed by polycationic peptides containing polyamine,[2] we used poly(ethylenimine) (PEI) that was preadsorbed into the cell walls of suspended cells of rice to induce in vitro silica formation under mild physiological conditions (pH 7.0) in the presence of tetramethyl orthosilicate (TMOS). An organic precursor to silicic acid (TMOS) was used to avoid the formation of precondensed solution-borne silicate colloids prior to wall surface nucleation.[29] In contrast to surfaces with the preadsorbed PEI, the cells in the absence of the PEI adsorption layer failed to induce surface silica nucleation on the walls

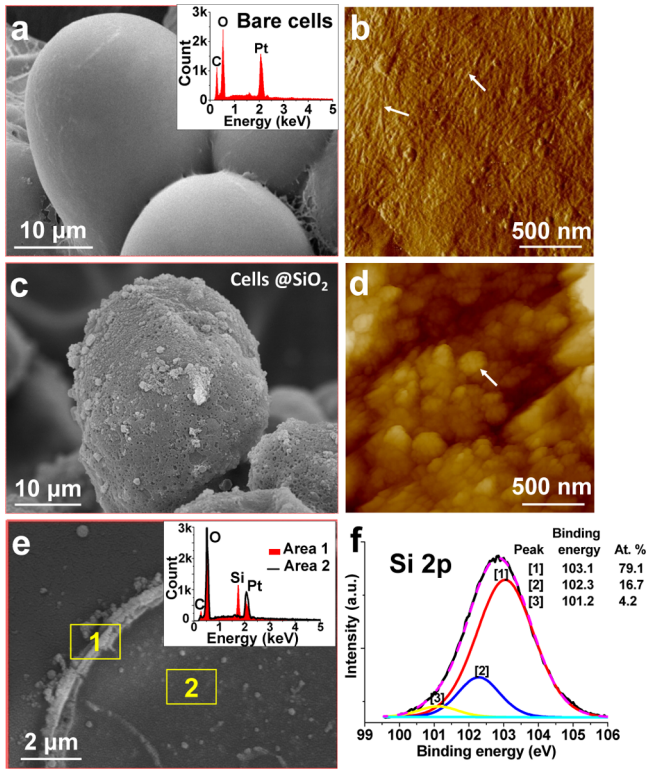

Figure 1. *Oryza sativa* cell surface coated with silica by bioinspired mineralization. (a) SEM and (b) corresponding AFM deflection image of the bare cell (uncoated) surface showing cellulose microfibrils (white arrows). (a, inset) energy-dispersive X-ray spectroscopy (EDX) highlighting the smooth surface in the absence of silica. (c) SEM and (d) AFM height image of silica-coated cell surface by preadsorbed poly(ethylenimine) (PEI) catalyzing in vitro silica formation, highlighting the rough surface of the silicified shell. A white arrow shows a silica nanoparticle. (e) SEM image of the cross-section of a cell and EDX (inset) showing the outermost layer of the rice cell was coated completely by a silica nanoshell with a thickness of 200−300 nm. (f) The Si 2p region of lyophilized cell walls was decomposed into three components at 103.1, 102.3, and 101.2 eV, suggesting the presence of inorganic and organic silicon species at the cell wall surface.

under identical solution conditions (Figure 1a), and the cellulose microfibrils of the cell wall were clearly visible and randomly oriented for all bare cells (Figure 1b). Following the silica encapsulation, the surface became uneven (Figure 1c) and was coated completely by silica nanoparticles with a relatively narrow size distribution (~90 nm in diameter) (Figure 1d and Figure S1). Each mesoporous nanoparticle is composed of 5 nm sized nanoparticles or even smaller with high surface areas (Figure S2). Energy-dispersive X-ray spectroscopy (EDX) indicated that these silica particles were mainly located in the cell walls (Figure S3), whereas the cytoplasm did not contain Si (Figure 1e). The sizes of the nanoparticles compared with the natural nanoparticles of amorphous silica are similar.[33,34]

The Si 2p core-level X-ray photoelectron spectroscopy (XPS) results of the coated cell walls show three components at 103.1, 102.3, and 101.2 eV (Figure 1f) corresponding to silica,[35] silicate/(poly)silicic acid,[35] and an unknown component, respectively. Our previous results have demonstrated that this unknown Si component is also present on the bare cell walls,[17] but its concentration is below the detection limit of EDX for the experimental conditions used; therefore, it was not measurable under EDX (Figure 1a, inset).

DOI: 10.1021/acssuschemeng.6b01736
ACS Sustainable Chem. Eng. 2016, 4, 6792−6799

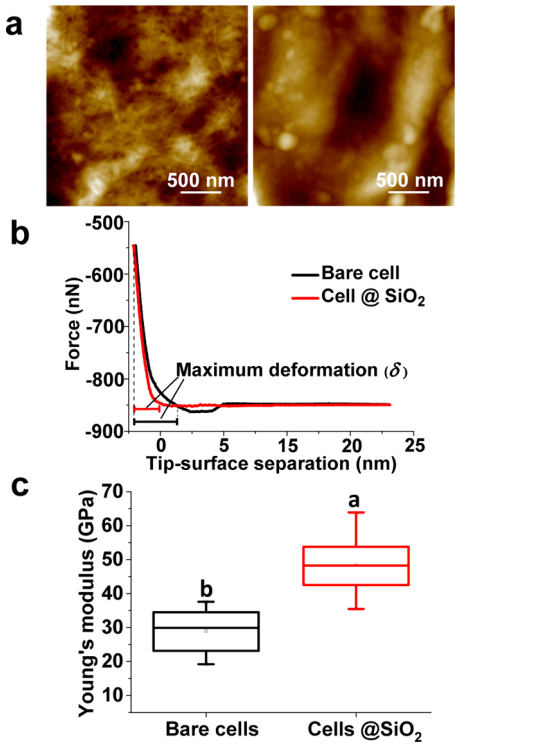

Figure 2. Mechanical properties of the bare and coated cells. (a) AFM height images of the bare (left) and coated (right) cell. (b) Force curve from AFM measurements showing a representation of the maximum deformation of a cell surface (δ) on which the Hertz model was applied to calculate the Young's modulus. (c) The Young's modulus E of the cell wall and the silica on the cell wall are approximately 29 and 48 GPa, respectively. Each value represents the average of 10 cells with 25 measurements per cell sample. Values are means ± SD. The horizontal lines of each box represent the 25th, 50th, and 75th percentile values, and the whiskers outside the box extend to the 5th and 95th percentile values. Different lowercase letters indicate a significant difference at $P < 0.05$.

The content of the peak at ~101.2 eV (4.2 at %) was much lower than the components at 103.1 (79.1 at %, silica) and 102.3 eV (16.7 at %, silicate or (poly)silicic acid) (Figure 1f).

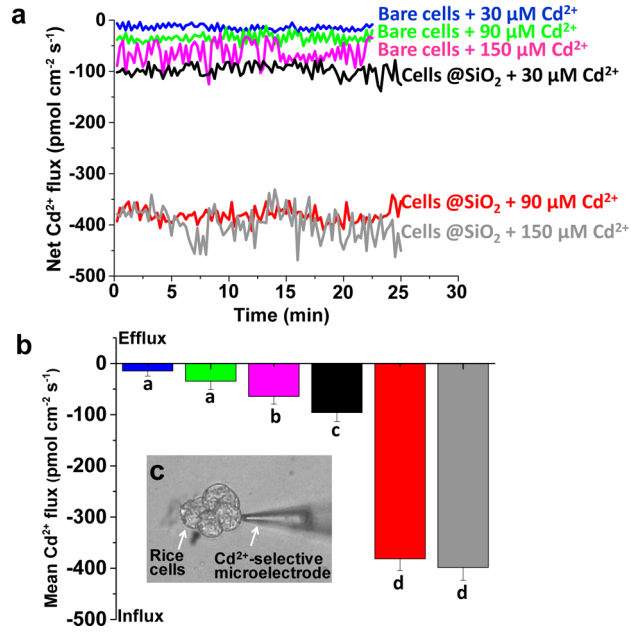

Figure 4. Cd^{2+} fluxes of rice cells in the absence and presence of silica nanoshells. (a) Kinetics of Cd^{2+} fluxes in bare and coated cells in the presence of 30, 90, or 150 μM Cd^{2+} in the measuring medium determined using in situ noninvasive microtest technology (NMT) as shown in (c) (arrows show representative cells and the Cd^{2+}-selective microelectrode). (b) The mean Cd^{2+} fluxes in corresponding cells using the mean value of six independent measurements (mean ± SD; $n = 6$). Different lowercase letters indicate significant difference at $P < 0.05$.

The Si_{2p} peak at 101.2 eV has been considered to be due to a Si−O−C or O−Si−C chemical environment:[17,36] 100.9 and 101.6 eV for Si−O $2p_{3/2}$ and Si−O $2p_{1/2}$, respectively, suggesting covalent bonding of Si with an organic long-chain molecule.[17,37] The peak positions of XPS shift to the higher energy from 100.1 to 101.2 eV, depending on the average coordination number of O atoms with Si atoms in Si−O−C bonds by organic ligands.[17,38] At present, we have no direct evidence for the nature of the interaction between Si and the

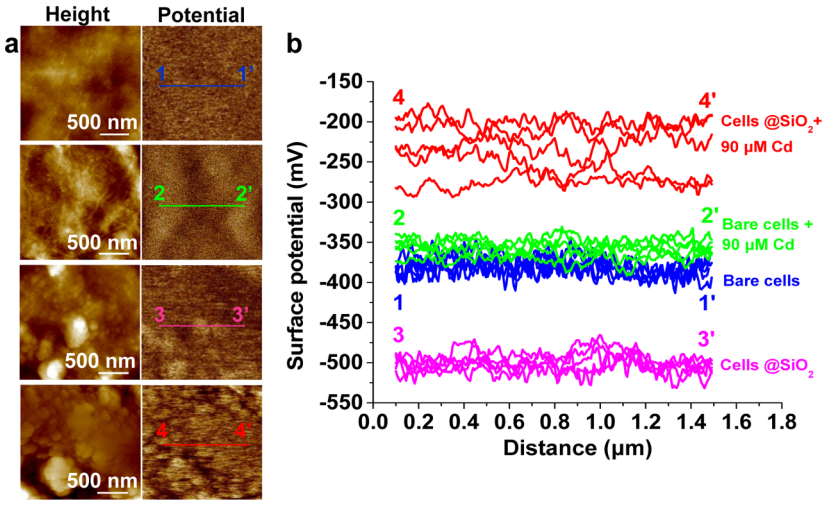

Figure 3. Surface potentials of the bare and coated rice cells before and after Cd adsorption. (a) Representative AFM height (left) and corresponding KPFM potential (right) images of the bare and coated cells before and after adsorbing 90 μM Cd^{2+}. (b) Surface potential distributions along lines 1 → 1′, 2 → 2′, 3 → 3′, or 4 → 4′ on the potential images in (a). Three different locations (lines in a) of 10 different surface samples were measured.

DOI: 10.1021/acssuschemeng.6b01736
ACS Sustainable Chem. Eng. 2016, 4, 6792−6799

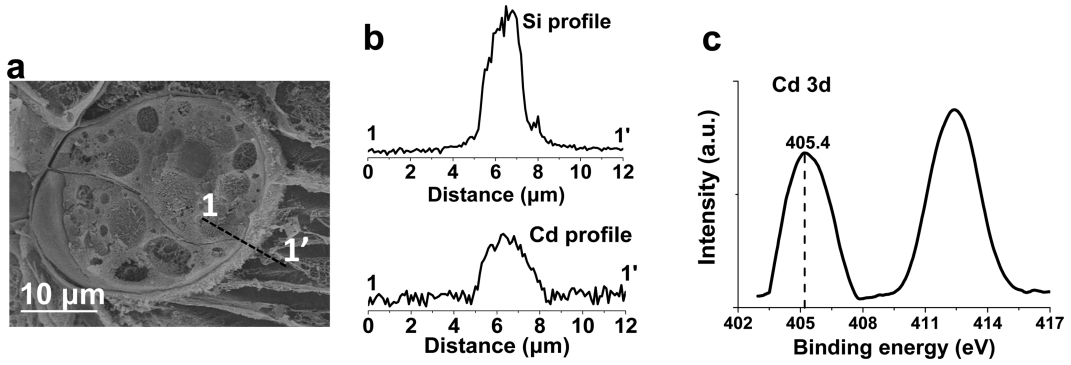

Figure 5. Elemental and binding state analyses of *Oryza* cells@SiO_2 after Cd^{2+} adsorption. (a) SEM image showing a cross-section of a cell@SiO_2 after adsorbing 90 μM $CdSO_4$. (b) The Si and Cd distributions by EDX along line 1 to 1′ in (a), showing that both Si and Cd distributed on the same locations of the walls. (c) XPS of Cd 3d for lyophilized cells@SiO_2, suggesting that only one oxidation state of Cd^{2+} was present on the silica shells.

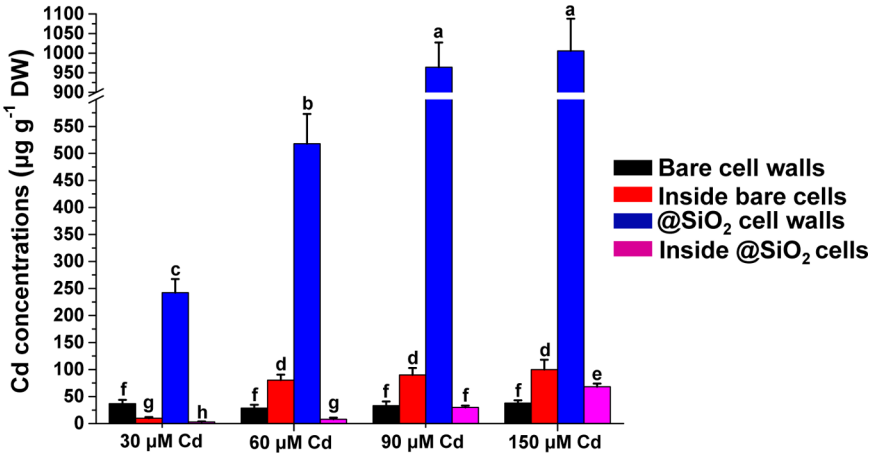

Figure 6. Cadmium (Cd) concentrations on cell walls and inside cells of bare and silica-coated rice (*Oryza sativa*) cells. Values are mean ± SD of three independent sets of experiments. Different lowercase letters indicate a significant difference at $P < 0.05$.

exact wall macromolecules (either in the form of polysaccharides or proteins or others) identified at the molecular level; thus, it is difficult to directly relate this XPS signal arising from the Si−O−C or O−Si−C or even Si−N linkage to an exact organic ligand on walls.[17,18]

Relative to the cell wall, the outer silica nanoshells might affect the mechanical robustness of the cell, which is critical to the light interception canopy architecture of rice leaves for higher photosynthesis efficiency. In fact, varieties like *japonica* type, which have a canopy of drooping leaves, produce lower biomass than those of the *indica-japonica* type with erect leaves.[39] To test this hypothesis, we investigated the mechanical behavior of the outer shell layer with atomic force microscopy (AFM) (Figure 2a). AFM nanoindentation showed that coated surfaces had a Young's modulus E of 48.3 ± 8.8 GPa, greater than 29.0 ± 8.6 GPa of uncoated cell surfaces (Figure 2b and c). The coated surfaces consist of inorganic silica particles associated with an organic wall matrix, which is consistent with observations of a comparable example of diatom silica with very strong deformation of the pleura of diatoms (2.5% strain, which causes, at E = 22.4 GPa, a stress of ∼560 N mm^{-2}), which elicited a completely elastic response,[40] i.e., the original shape of diatom shells is regained when the pressure is removed. Yamanaka et al. have shown that silica structures in the epidermis of rice leaves inhibit leaves from undergoing twisting torsions, which may assist the leaves in absorbing sunlight more effectively for photosynthesis.[41] It has also been suggested that the increased silicification of bulliform cells and the cell walls of long cells should translate to greater mechanical strength.[42] Within wetland plants, an obvious relationship exists between cellulose of the cell wall and silica to promote different strengthening strategies.[43] Clearly, the silicified structures in rice have evolved to withstand external pressure, and considerable energy for bending is required by which lodging in rice occurs in a more closely planted population.[15]

As the silica nanoparticles contain an amorphous network of tetrahedral SiO_4 inside and abundant Si−OH groups at the outer surface, more negatively charged SiO^- are dissociated from Si−OH groups, resulting in higher negative surface charge density across a range of pH values.[44] The local surface charge depends on the particle size and electrolyte solution properties.[44] The magnitude of surface charge increases with a decrease in the particle size.[44] This may serve to adsorb more metal ions from solution than the cell wall alone. The surface potential and adsorption performance of aqueous metal cations onto cell walls and silica nanoshells formed on the walls was investigated with both AFM in Kelvin probe mode (KPFM) and in situ noninvasive microtest technology (NMT). First, we investigated the surface potentials of the cell wall and silica nanoshell on the wall using KPFM, exhibiting −380 ± 40 and −500 ± 30 mV, respectively (Figure 3). This demonstrates a greater negative charged surface present in the silica nanoshell

DOI: 10.1021/acssuschemeng.6b01736
ACS Sustainable Chem. Eng. 2016, 4, 6792−6799

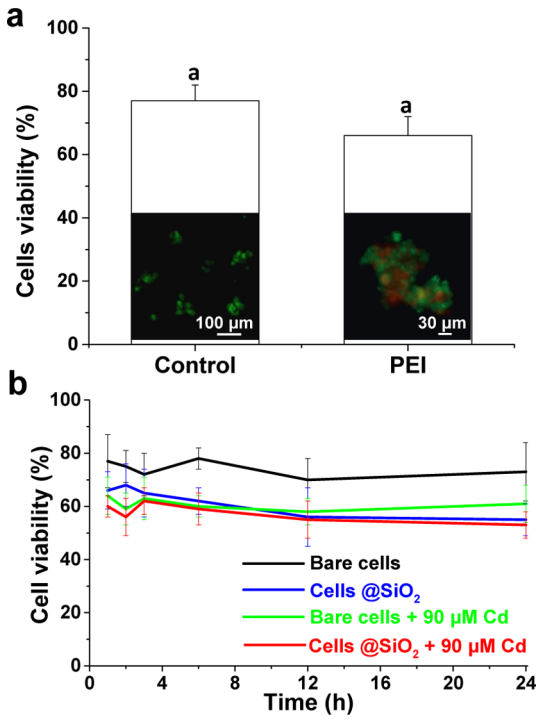

Figure 7. Cell viability measured by FDA-PI staining. (a) Viability of bare cells (uncoated cells as control) and cells preadsorbed with PEI. Insets in columns are light microscopy images showing living cells (green) and dead cells (red). (b) Viability change with treatment time for bare cells, cells@SiO_2, bare cells treated with 90 μM Cd, and cells@SiO_2 treated with 90 μM Cd. The experiment was repeated three times, and more than 100 cells were observed in each treatment.

than the wall alone. The surface potential distribution was significantly decreased to -240 ± 60 mV for silica nanoshells with the addition of 90 μM Cd^{2+} ions (Figure 3), whereas no obvious changes in surface potential were observed for the cell walls at the same concentration of Cd (Figure 3).

The kinetics of Cd^{2+} ion uptake by the unsilicified and silicified cells was determined by in situ measuring the Cd^{2+} ion influxes F using NMT, and the values of F of 14.6, 34.7, and 64.4 pmol cm^{-2} s^{-1} obtained for bare cells are significantly less than the 95.9, 381.4, and 398.5 pmol cm^{-2} s^{-1} for coated cells adsorbing 30, 90, or 150 μM Cd^{2+}, respectively (Figure 4), indicating that coated cells removed Cd^{2+} ions from solution much more quickly than bare cells prior to reaching their equilibrium uptake. This near-instantaneous adsorption of Cd ions by the silica nanoshells is attributable to their higher surface potential (Figure 3), most likely due to their higher surface area and porosity. Moreover, after sectioning cells by low-temperature microtoming (Figure 5a), the elemental distribution profiles of the Si and Cd analyzed by EDX confirmed that Cd is mainly present on the silicified cell walls (Figure 5b). XPS results of Cd $3d_{5/2}$ at 405.4 eV (Figure 5c) further indicated that Cd ions are adsorbed and accumulated through surface complexation as $(SiO^-)_2Cd$ from deprotonated Si−OH species.[45] This symmetrical peak at 405.4 eV suggests that only one oxidation state of Cd^{2+} is present on the silica shells.[46] Furthermore, we reasonably reckoned intracellular Cd contents according to both of our previous measurements[25,26] and the present NMT results (Figure 4), further demonstrating a significant inhibition of Cd uptake into cells by the silicified cell walls (Figure 6). These results explained the outcome of previous experiments in which rice was able to enhance Cd tolerance following Si application.[47]

The cell walls typically carry a number of negatively charged groups such as carboxyl and hydroxyl that generate a net electrostatic field, which may influence the partitioning of Cd^{2+} ions.[48] Rice suspension cells have a primary cell wall that is composed of polysaccharides (pectins, hemicelluloses, and cellulose) and smaller proportions of glycoproteins.[49] Our previous results showed that the cell walls possessed substantial Cd-binding capacity.[26] However, as the Cd concentration increases (>30 μM), the Cd binding and adsorption sites in the cell walls reach saturation, thus allowing an increased Cd uptake into the cells.[26] Following silicification, the silica shells exert a significant influence on Cd sequestration at environmentally relevant concentrations, an important defensive measure in protecting cells from heavy metal Cd poisoning. Finally, we noticed that after PEI and silica coating, the viability of cells decreased slightly to ~56−66% from ~77% (Figure 7a), suggesting that adverse effects of coating on cells should be present. In addition, more than 60% of cells, regardless of the absence or presence of silica shells, were viable after Cd exposure for 24 h at a normal growth temperature (Figure 7b). The most likely explanation is the homeostatic regulation by which excess Cd^{2+} ions in the medium rapidly activate various cell response mechanisms in the unsilicified cells,[50] whereas the silicified cells survive by the rapid removal of Cd^{2+} ions from solution using silica nanoshells.

Silicon cycles between the *Poaceae* plants and the environment,[51] although the absolute requirement of silicon for plant survival continues to be debated.[52] Intra- or extracellular silicification of rice plants can significantly alleviate a range of abiotic stresses, including heavy metal toxicity and lodging,[15,53] consequently improving plant growth and yield by increasing light interception, leaf erectness, and stem hardness.[54−58] However, the mechanism of action of biosilicification is largely overlooked due to its multiscale complexity at the tissue, organ, and whole-plant level. The present single-cell study provides an innovative method for in situ evaluation of the relative effectiveness of structural silica in heavy metal Cd sequestration and detoxification and costs of using either carbon- or silicon-based support for plant strength, although this artificial system does not accurately mimic the natural one.

CONCLUSIONS

It is now possible to use the single-cell system developed here to determine how the response and behavior of individual cells depend on the extent of silicification and how silicification provides additional capabilities at various biological contexts. More generally, this approach should help us to augment the ability to determine the role of silica at the single-cell level. Results showed a multifunctionality of the silicified cell walls with an enhanced cell strength and a capability to inhibit cadmium ion uptake into the cells. The multifunctional extracellular biosilicification may have had significant influence in rice growth and the biogeochemical cycle of silicon over the course of its evolutionary history. It is conceivable that all whole-plant phenomena in silicon studies are explained mechanistically according to surface physical and chemical properties of amorphous silica formed on the cell walls, which are responsible for the role of silicified structures in a plant consisting of various individual cells.

DOI: 10.1021/acssuschemeng.6b01736
ACS Sustainable Chem. Eng. 2016, 4, 6792−6799

■ ASSOCIATED CONTENT

Supporting Information

The Supporting Information is available free of charge on the ACS Publications website at DOI: 10.1021/acssuschemeng.6b01736.

The composition for AA medium (Table S1), nanoparticle size of the silica shells of cells @SiO_2 (Figure S1), surface morphology of cells @SiO_2 (Figure S2), and Si elemental mapping (Figure S3) (PDF)

■ AUTHOR INFORMATION

Corresponding Author

*E-mail: ljwang@hzau.edu.cn.

Notes

The authors declare no competing financial interest.

■ ACKNOWLEDGMENTS

This work was supported by the National Natural Science Foundation of China (Grant 31172027) and the Fundamental Research Funds for the Central Universities (2662015PY206). We thank Dr. Richard Gordon for careful reading of the manuscript.

■ REFERENCES

(1) Keilin, D. The Leeuwenhoek Lecture—the Problem of Anabiosis or Latent Life—History and Current concept. *Proc. R. Soc. London, Ser. B* **1959**, *150*, 149−191.

(2) Kröger, N.; Deutzmann, R.; Sumper, M. Polycationic Peptides from Diatom Biosilica that Direct Silica Nanosphere Formation. *Science* **1999**, *286*, 1129−1132.

(3) Kröger, N.; Lorenz, S.; Brunner, E.; Sumper, M. Self-Assembly of Highly Phosphorylated Silaffins and Their Function in Biosilica Morphogenesis. *Science* **2002**, *298*, 584−586.

(4) Sumper, M. A Phase Separation Model for the Nanopatterning of Diatom Biosilica. *Science* **2002**, *295*, 2430−2433.

(5) Park, J. H.; Yang, S. H.; Lee, J.; Ko, E. H.; Hong, D.; Choi, I. S. Nanocoating of Single Cells: from Maintenance of Cell Viability to Manipulation of Cellular Activities. *Adv. Mater.* **2014**, *26*, 2001−2010.

(6) Liu, Z.; Xu, X. R.; Tang, R. K. Improvement of Biological Organisms Using Functional Material Shells. *Adv. Funct. Mater.* **2016**, *26*, 1862−1880.

(7) Xu, X. R.; Wang, B.; Tang, R. K. Hybrid Materials that Integrate Living Cells: Improved Eco-Adaptation and Environmental Applications. *ChemSusChem* **2011**, *4*, 1439−1446.

(8) Park, J. H.; Hong, D.; Lee, J.; Choi, I. S. Cell-in-Shell Hybrids: Chemical Nanoencapsulation of Individual Cells. *Acc. Chem. Res.* **2016**, *49*, 792−800.

(9) Wang, G.; Wang, L. J.; Liu, P.; Yan, Y.; Xu, X.; Tang, R. K. Extracellular Silica Nanocoat Confers Thermotolerance on Individual Cells: A Case Study of Material-Based Functionalization of Living Cells. *ChemBioChem* **2010**, *11*, 2368−2373.

(10) Lee, J.; Choi, J.; Park, J. H.; Kim, M. H.; Hong, D.; Cho, H.; Yang, S. H.; Choi, I. S. Cytoprotective Silica Coating of Individual Mammalian Cells through Bioinspired Silicification. *Angew. Chem., Int. Ed.* **2014**, *53*, 8056−8059.

(11) Vaughan, D. A.; Morishima, H.; Kadowaki, K. Diversity in the Oryza Genus. *Curr. Opin. Plant Biol.* **2003**, *6*, 139−146.

(12) Uraguchi, S.; Mori, S.; Kuramata, M.; Kawasaki, A.; Arao, T.; Ishikawa, S. Root-to-shoot Cd Translocation Via the Xylem is the Major Process Determining Shoot and Grain Cadmium Accumulation in Rice. *J. Exp. Bot.* **2009**, *60*, 2677−2688.

(13) Sanita di Toppi, L.; Gabbrielli, R. Response to Cadmium in Higher Plants. *Environ. Exp. Bot.* **1999**, *41*, 105−130.

(14) Nawrot, T. S.; Staessen, J. A.; Roels, H. A.; Munters, E.; Cuypers, A.; Richart, T.; Ruttens, A.; Smeets, K.; Clijsters, H.; Vangronsveld, J. Cadmium Exposure in the Population: From Health Risks to Strategies of Prevention. *BioMetals* **2010**, *23*, 769−782.

(15) Idris, M.; Hossain, M. M.; Choudhury, F. A. The Effect of Silicon on Lodging of Rice in Presence of Added Nitrogen. *Plant Soil* **1975**, *43*, 691−695.

(16) Chu, C. C. Establishment of an Efficient Medium for Anther Culture of Rice through Comparative Experiments on the Nitrogen Sources. *Scientia Sinica* **1975**, *18*, 659−668.

(17) He, C. W.; Wang, L. J.; Liu, J.; Liu, X.; Li, X. L.; Ma, J.; Lin, Y. J.; Xu, F. S. Evidence for 'Silicon' within the Cell Walls of Suspension-Cultured Rice Cells. *New Phytol.* **2013**, *200*, 700−709.

(18) He, C. W.; Ma, J.; Wang, L. J. A Hemicellulose-Bound Form of Silicon with Potential to Improve the Mechanical Properties and Regeneration of the Cell Wall of Rice. *New Phytol.* **2015**, *206*, 1051−1062.

(19) Pletikapić, G.; Berquand, A.; Radić, T. M.; Svetličić, V. Quantitative Nanomechanical Mapping of Marine Diatom in Seawater using Peak Force Tapping Atomic Force Microscopy. *J. Phycol.* **2012**, *48*, 174−185.

(20) Kuznetsova, T. G.; Starodubtseva, M. N.; Yegorenkov, N. I.; Chizhik, S. A.; Zhdanov, R. I. Atomic Force Microscopy Probing of Cell Elasticity. *Micron* **2007**, *38*, 824−833.

(21) Chanliaud, E.; Burrows, K. M.; Jeronimidis, G.; Gidley, M. J. Mechanical Properties of Primary Plant Cell Wall Analogues. *Planta* **2002**, *215*, 989−996.

(22) Fujihira, M. Kelvin Probe Force Microscopy of Molecular Surfaces. *Annu. Rev. Mater. Sci.* **1999**, *29*, 353−380.

(23) Leung, C.; Kinns, H.; Hoogenboom, B. W.; Howorka, S.; Mesquida, P. Imaging Surface Charges of Individual Biomolecules. *Nano Lett.* **2009**, *9*, 2769−2773.

(24) Tsai, C. C.; Hung, H. H.; Liu, C. P.; Chen, Y. T.; Pan, C. Y. Changes in Plasma Membrane Surface Potential of PC12 Cells as Measured by Kelvin Probe Force Microscopy. *PLoS One* **2012**, *7*, e33849.

(25) Ma, J.; Cai, H. M.; He, C. W.; Zhang, W. J.; Wang, L. J. A Hemicellulose-Bound Form of Silicon Inhibits Cadmium Ion Uptake in Rice (*Oryza sativa*) Cells. *New Phytol.* **2015**, *206*, 1063−1074.

(26) Liu, J.; Ma, J.; He, C. W.; Li, X. L.; Zhang, W. J.; Xu, F. S.; Lin, Y. J.; Wang, L. J. Inhibition of Cadmium Ion Uptake in Rice (*Oryza sativa*) Cells by a Wall-Bound Form of Silicon. *New Phytol.* **2013**, *200*, 691−699.

(27) Bai, L.; Ma, X.; Zhang, G.; Song, S.; Zhou, Y.; Gao, L.; Miao, Y.; Song, C. P. A Receptor-Like Kinase Mediates Ammonium Homeostasis and Is Important for the Polar Growth of Root Hairs in *Arabidopsis*. *Plant Cell* **2014**, *26*, 1497−1511.

(28) Exley, C. Silicon in Life: Whither Biological Silicification? In *Biosilica in Evolution, Morphogenesis and Nanobiotechnology*; Müller, W. E. G., Grachev, M. A., Eds.; Springer-Verlag: Berlin, Heidelberg, 2009; Vol. *47*, pp 173−184.

(29) Wallace, A. F.; De Yoreo, J. J.; Dove, P. M. Kinetics of Silica Nucleation on Carboxyl- and Amine-Terminated Surfaces: Insights for Biomineralization. *J. Am. Chem. Soc.* **2009**, *131*, 5244−5250.

(30) Casey, W. H.; Kinrade, S. D.; Knight, C. T. G.; Rains, D. W.; Epstein, E. Aqueous Silicate Complexes in Wheat *Triticum aestivum* L. *Plant, Cell Environ.* **2004**, *27*, 51−54.

(31) Exley, C. A Possible Mechanism of Biological Silicification in Plants. *Front. Plant Sci.* **2015**, *6*, 853.

(32) Carpita, N. C. Strcuture and Biogenesis of the Cell Walls of Grasses. *Annu. Rev. Plant Physiol. Plant Mol. Biol.* **1996**, *47*, 445−476.

(33) Wang, L. J.; Wang, Y.; Chen, Q.; Cao, W.; Li, M.; Zhang, F. S. Silicon Induced Cadmium Tolerance of Rice Seedlings. *J. Plant Nutr.* **2000**, *23*, 1397−1406.

(34) Wang, L. J.; Nie, Q.; Li, M.; Zhang, F. S.; Zhuang, J. Q.; Yang, W. S.; Li, T. J.; Wang, Y. H. Biosilicified Structures for Cooling Plant Leaves: A Mechanism of Highly Efficient Midinfrared Thermal Emission. *Appl. Phys. Lett.* **2005**, *87*, 194105.

(35) Tesson, B.; Genet, M. J.; Fernandez, V.; Degand, S.; Rouxhet, P. G.; Martin- Jézéquel, V. Surface Chemical Composition of Diatoms. *ChemBioChem* **2009**, *10*, 2011−2024.

DOI: 10.1021/acssuschemeng.6b01736
ACS Sustainable Chem. Eng. 2016, 4, 6792−6799

(36) Boukherroub, R.; Morin, S.; Sharpe, P.; Wayner, D. D.; Allongue, P. Insights into the Formation Mechanisms of Si-OR Monolayers from the Thermal Reactions of Alcohols and Aldehydes with Si(111)-H. *Langmuir* **2000**, *16*, 7429−7434.
(37) Effenberger, F.; Götz, G.; Bidlingmaier, B.; Wezstein, M. Photoactivated Preparation and Patterning of Self-Assembled Monolayers with 1-alkenes and Aldehydes on Silicon Hydride Surfaces. *Angew. Chem., Int. Ed.* **1998**, *37*, 2462−2464.
(38) Nakayama, H.; Hata, T. Low-Temperature Growth of Si-Based Organic-Inorganic Hybrid Materials Si-O-C and Si-N-C by Organic Cat-CVD. *Thin Solid Films* **2006**, *501*, 190−194.
(39) Xu, Y.; This, D.; Pausch, R. C.; Vonhof, W. M.; Coburn, J. R.; Comstock, J. P.; McCouch, S. R. Leaf-Level Water Use Efficiency Determined by Carbon Isotop Discrimination in Rice Seedlings: Genetic Variation Associated with Population Structure and QTL Mapping. *Theor. Appl. Genet.* **2009**, *118*, 1065−1081.
(40) Hamm, C. E.; Merkel, R.; Springer, O.; Jurkojc, P.; Maier, C.; Prechtel, K.; Smetacek, V. Architecture and Material properties of Diatom Shells Provide Effective Mechanical Protection. *Nature* **2003**, *421*, 841−843.
(41) Yamanaka, S.; Takeda, H.; Komatsubara, S.; Ito, F.; Usami, H.; Togawa, E.; Yoshino, K. Structures and Physiological Functions of Silica Bodies in the Epidermis of Rice Plant. *Appl. Phys. Lett.* **2009**, *95*, 123703.
(42) Kaufman, P. B.; Dayanandan, P.; Franklin, C. I.; Takeoka, Y. Structure and Function of Silica Bodies in the Epidermal System of Grass Shoots. *Ann. Bot.* **1985**, *55*, 487−507.
(43) Schoelynck, J.; Bal, K.; Backx, H.; Okruszko, T.; Meire, P.; Struyf, E. Silica Uptake in Aquatic and wetland Macrophytes: A Strategic Choice between Silica, Lignin and Cellulose? *New Phytol.* **2010**, *186*, 385−391.
(44) Barisik, M.; Atalay, S.; Beskok, A.; Qian, S. Size Dependent Surface Charge Properties of Silica Nanoparticles. *J. Phys. Chem. C* **2014**, *118*, 1836−1842.
(45) Tan, G. Q.; Xiao, D. Adsorption of Cadmium Ion from Aqueous Solution by Ground Wheat Stems. *J. Hazard. Mater.* **2009**, *164*, 1359−1363.
(46) Gulino, A.; Dapporto, P.; Rossi, P.; Fragala, I. Synthesis and Characterization of Liquid MOCVD Precursors for Thin Films of Cadmium oxide. *Chem. Mater.* **2002**, *14*, 4955−4962.
(47) Zhang, C. C.; Wang, L. J.; Nie, Q.; Zhang, W. X.; Zhang, F. S. Long-Term Effects of Exogenous Silicon on Cadmium Translocation and Toxicity in Rice (*Oryza sativa L.*). *Environ. Exp. Bot.* **2008**, *62*, 300−307.
(48) Duval, J. F. L.; van Leeuwen, H. P. Rates of Ionic Reactions with Charged Nanoparticles in Aqueous Media. *J. Phys. Chem. A* **2012**, *116*, 6443−6451.
(49) Fry, S. C. Primary Cell Wall Metabolism: Tracking the Careers of Wall Polymers in Living Plant Cells. *New Phytol.* **2004**, *161*, 641−675.
(50) Hall, J. L. Cellular Mechanisms for Heavy Metal Detoxification and Tolerance. *J. Exp. Bot.* **2002**, *53*, 1−11.
(51) Conley, D. J.; Carey, J. C. Silica Cycling over Geological Time. *Nat. Geosci.* **2015**, *8*, 431−432.
(52) Cooke, J.; Leishman, M. R. Is Plant Ecology More Siliceous Than We Realise? *Trends Plant Sci.* **2011**, *16*, 61−68.
(53) Neumann, D.; zur Nieden, U. Silicon and Heavy Metal Tolerance of Higher Plants. *Phytochemistry* **2001**, *56*, 685−692.
(54) Ma, J. F.; Tamai, K.; Yamaji, N.; Mitani, N.; Konishi, S.; Katsuhara, M.; Ishiguro, M.; Murata, Y.; Yano, M. A Silicon Transporter in Rice. *Nature* **2006**, *440*, 688−691.
(55) Ando, H.; Kakuda, K. I.; Fujii, H.; Suzuki, K.; Ajiki, T. Growth and Canopy Structure of Rice Plants Grown under Field Conditions as Affected by Si Application. *Soil Sci. Plant Nutr.* **2002**, *48*, 429−432.
(56) Epstein, E. The Anomaly of Silicon in Plant Biology. *Proc. Natl. Acad. Sci. U. S. A.* **1994**, *91*, 11−17.
(57) Epstein, E. Silicon. *Annu. Rev. Plant Physiol. Plant Mol. Biol.* **1999**, *50*, 641−664.
(58) Liang, Y. C.; Nikolic, M.; Bélanger, R.; Gong, H. J.; Song, A. *Silicon in Agriculture From Theory to Practice*; Springer: New York, 2015.

DOI: 10.1021/acssuschemeng.6b01736
ACS Sustainable Chem. Eng. 2016, 4, 6792−6799